



The experimental study of the expert system for diagnosing unbalances by ANN and acoustic signals

Wenlung Li^{a,*}, Y.P. Tsai^b, C.L. Chiu^b

^a*Department of Mechanical Engineering, National Taipei University of Technology, Chung Hsiao E Road, Taipei 10626, Taiwan*

^b*Institute of Manufacturing Tech, National Taipei University of Technology, Taipei, Taiwan*

Received 1 August 2002; accepted 20 March 2003

Abstract

The expert system based on the backward propagation neural network (BPN) has been developed and tested for diagnosing mass unbalance of rotational machines. The system adopts the acoustic signals as input features. In order to minimize the distance and background noise effects, the so-called *d*-normalization was introduced. The *d*-normalization is similar to the loudness in speech synthesis. By utilizing the normalized power spectra together with the rectified statistic moments of higher order of the acoustic signals, the system is found to be very successful. However, it was found that the system still could not discriminate those faults near the natural frequencies. The main reason may stem from the system non-linearities even though they are small.

© 2003 Elsevier Ltd. All rights reserved.

1. Introduction

Generally speaking, an expert system is a software package containing at least a knowledge base, a reasoning unit and man–machine interfaces. Depending on the reasoning unit, there exist many different types of expert systems. For example, Drake and Pan [1] use a neural network system to monitor the transient responses for the coolant system of a machine tool. The report showed that the fault classification ability was good in multi-fault monitoring with correct classification rate of 100%. For long-term monitoring, they reported the correct classification rate of 30%. In addition, a neural network-based expert system was applied to diagnose the defects of

*Corresponding author. Tel.: +886-22771-2171-2023; fax: +886-2-2731-7191.

E-mail address: wlli@ntut.edu.tw (W. Li).

roller bearings [2–5]. They [3] reported that the system has the ability to identify different defects with correct classification rate of 94%. For other review papers, one can refer to excellent papers such as e.g., [6,7].

In fact, a diagnosis system is indeed a kind of pattern recognition. No matter which type of expert system is chosen, one key factor that affects the system results is the sensors. The sensor detects the physical changes of the machine or parts, and the signals are then transduced to and stored in the computer for the expert system. Therefore, the quality that a sensor can attain surely changes the results of an artificial neural network (ANN) system. Normally, sensors that are directly mounted onto the machine are commonly used. This type of sensor includes, for example, proximity probes which sense the displacement changes, and accelerometers which sense the acceleration changes of an object. However, they need to be mounted directly on fixed parts. Thus, such sensors may cause certain inconveniences especially for those machines that do not provide appropriate locations for mounting such sensors. In addition, those sensors may be contaminated and operators may not notice them. Even worse, one has no way of knowing a priori the locations where good quality signals can be appropriately acquired so that sensors can be mounted at the right places.

The alternative way may be to select sensors that do not need to be mounted on the part. In practice, this type of sensor includes two categories. The first one is the laser sensor [8]. Although laser sensors can be used to detect signals of high frequency, they are somewhat more expensive. The second category may be the acoustic sensors or microphones. Unfortunately, the background noise is often a big problem for this type of sensor.

The objective of the present report is to develop an expert system for a rotating machine. The faults include mass unbalance, shaft-bow misalignment, and looseness, etc. In addition, the acoustic signals are the major considerations for the ANN inputs. However, it has been shown [9] that the latter two are not sensitive enough to the microphone sensor. They will not be included in the present report. Readers may directly refer to Chiu [9] for further discussions.

2. The neural network

Clearly, certain malfunctions of rotary machines may be diagnosed through the vibrations of the machine. However, it is not an easy task because there is no simple normal/malfunction relationship. As a consequence, a computer-aided expert system like an ANN may be right answer to this problem.

For an artificial expert system, reliability and applicability are the two most important factors to be taken into consideration even at the first stage of development. However, the input signals obtained from fields are always contaminated or incomplete. Therefore, the backward propagation network (BPN) neural network model that has been applied and reported well in industries is selected for the present investigation. And, its parameters and input features have to be set and tested using the acoustic microphone as the input sensor. However, for comparison, signals of proximity probes have also been added where they are necessary.

In general, the application of BPN algorithm, as shown in Fig. 1(a), involves the calculation of the error between the network output vector and the target vector. Let the BPN have the input vector \mathbf{x} of length N_{in} , the network output vector \mathbf{y} of length r , and the synaptic weight matrix \mathbf{W} .

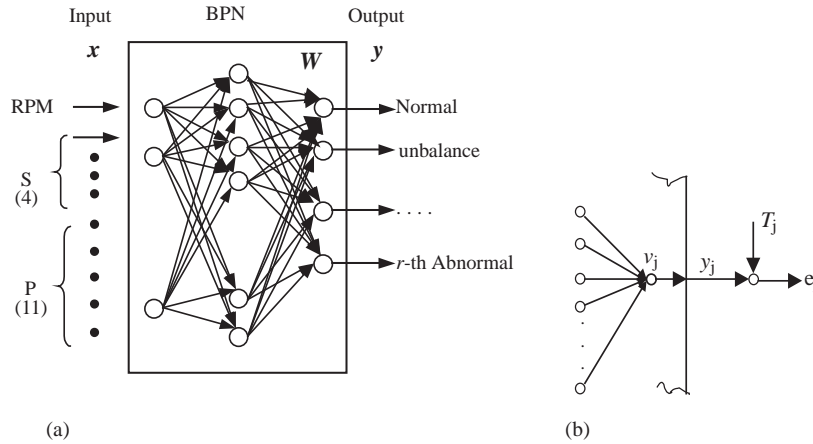


Fig. 1. (a) Schematic diagram of the diagnosis system. (b) The output error of the BPN.

Then a transfer function f maps \mathbf{x} into \mathbf{y} by

$$\mathbf{y} = f(\mathbf{W}^T \mathbf{x} - \theta) = f(\mathbf{v}), \tag{1}$$

where θ is the bias that is used to mimic the threshold value of the axon, below which the neuron would not respond, \mathbf{v} the output net activity vector. For BPN with a supervised learning process, there exist two distinct computation passes. The first one is referred to as the ‘forward pass’ in which the synaptic weight matrix remains unchanged. In other words, the information inputs pass forward to the output. On the other hand, the second pass is called the ‘backward pass’ where the error is passing backwards starting from the outermost layer. Thus, through the recursive computation for each neuron the weight matrix undergoes modifications. Or, let the $(n + 1)$ th change of weight matrix be $\mathbf{W}(n + 1)$. Then

$$\mathbf{W}(n + 1) = \mathbf{W}(n) + \Delta \mathbf{W}(n), \tag{2}$$

where $\Delta \mathbf{W}(n)$ is the weight adjustment matrix obtained from the last change. And the correction value of node from i th to j th is

$$\Delta W_{ji}(n) = \eta \cdot \delta_j(n) y_i(n) + \alpha \Delta W_{ji}(n - 1), \tag{3}$$

where η , α and δ_j are the learning rate, the momentum constant [10] and the local gradient, respectively. Since the sigmoid function is chosen as the transfer function, refer to Fig. 1(b), the local gradient δ_j of the j th node and the output error vector \mathbf{e} , which is the Euclidean distance of the target vector \mathbf{T} and the output vector \mathbf{v} , are related by the expression

$$\delta_j(n) = e_j(n) \cdot f'(v_j(n)), \tag{4}$$

or [11]

$$\delta_j = \begin{cases} y_j(n)[1 - y_j(n)] \sum_k \delta_k W_{kj}(n), \\ [T_j(n) - y_j(n)] y_j(n)[1 - y_j(n)]. \end{cases} \tag{5}$$

The former of Eq. (5) is good for the non-output or hidden layers, while the latter for the output layer, respectively. Besides, the subscripts of W_{kj} denote the weighting factor of the BPN

from node j to k . Readers are referred to BPN books such as e.g., [11] for more details on derivations.

On the other hand, the choice for the initial weights is one other crucial factor that affects the convergence of the ANN. In general, the wrong starting weights can always delay the convergence speed. For example, the possibility that the ANN converges to a local optimal, instead of the global one, gets much higher in case excessively when large initial weights are given. That is because the BPN may be saturated too quickly. In order to avoid this situation, the initial weights were selected as uniform random real numbers in $[-0.5, +0.5]$ for the current ANN. Furthermore, the number of neurons of the hidden layer has been set to be $N_H = (N_{in} + r)/2$, where N_{in} is the number of feature inputs, r the number of output vectors or the dimension of \mathbf{y} .

The other network parameters like the learning rate, momentum, number of hidden layers, the number of nodes for the individual hidden layer, etc., are also important and have been discussed by many researchers, e.g., [12]. However, for the present study, such network parameters are simply picked in such a way that the BPN reasonably converges in the training process. For example, to choose a value for the learning rate can be crucial and different algorithms with different advantages are given in Ref. [12]. For the current case, the initial learning rate is simply set to 3.0 and with decreasing rate of 95% to the minimum learning rate of 0.2 [9]. In addition, the learning momentum is set with the same decreasing rate of 95% and minimum value as the learning rate but a different initial momentum value of 0.95. These values are believed to be reasonable and have been tested and verified before being put into the system.

The stop criterion of convergence for the network is set to the cumulative maximum error, ε_{max} , smaller than 0.2%. The cumulative maximum error of N training samples is defined as follows

$$\varepsilon_{max} = \frac{1}{2N} \sum_{n=1}^N \frac{\|\mathbf{y} - \mathbf{T}\|^2}{r}, \quad (6)$$

where \mathbf{y} denotes the estimated output vector of the network and \mathbf{T} the known target vector of the training samples.

3. Input signals

All rotating machinery tends to generate periodic signals no matter whether it is in normal or malfunction condition. The most common way to understand these signals is through its vibrations and sound. Independent of the ways of signal they certainly relate to various physical characteristics. On the other hand, these signals may be classified into two categories. Depending on their representation, they can be either in the time or in the frequency domains. However, most field engineers prefer to have their signals transformed into the latter [13]. That is, the detected time-domain signals are transformed into frequency signals by using an FFT algorithm. Using this frequency signal, as has been shown in Ref. [13], most malfunctions, namely, mass unbalance, misalignment, looseness, and axis bent, etc., can be successfully diagnosed with the aid of the ANN, if the signals used in it honestly represent the machine. For the signal treatments in the frequency domain, readers are referred to [13] for detail.

However, any signal in the frequency domain has to be acquired from the time domain a priori. And all directly acquired signals include as much noise error as information. As a consequence,

the choice of signal representation must be as robust as possible. Here, ‘robust’ means ‘insensitive to noise or other uncontrollable parameters.’ As indicated in many research reports, there exist many choices for the signal representations. Among them, it has adopted the statistical moments [13] as one of the input signals for the current ANN. That is, the n th moments of a random variable $X(t)$ about an arbitrary point k are defined by [14,15]

$$E[(x - k)^n] = \int_{-\infty}^{\infty} (x - k)^n \cdot f_X(x) dx, \tag{7}$$

or

$$M_n = E[(x - k)^n] \cong \sum_{i=1}^N (x_i - k)^n \cdot p(x_i), \tag{8}$$

in which $E[\cdot]$ denotes the expectation, $f_X(x)$ is the probability density function (PDF) of X , N total number of points. It is worth of note that Eq. (7) is obviously for a continuous random variable while Eq. (8) is for a discrete one. In case the moments are calculated with respect to the first moment or mean value, μ_X , i.e., $k = \mu_X$, the second statistical moment ($n = 2$) is the well-known variance of X or σ_X^2 . In general, all higher moments normalized about μ_X are the central statistical moments, i.e.,

$$\mu_X = \frac{1}{N} \sum_{i=1}^N x_i. \tag{9}$$

Furthermore, the third and fourth moments are called the skewness and kurtosis coefficients, respectively, after their physical meanings in PDF. That is, let S_X and κ_X be the skewness and kurtosis of X . Then they are defined by

$$S_X = \frac{M_3}{\sigma_X^3} = \frac{E[(x - \mu_X)^3]}{\sigma_X^3}, \tag{10}$$

and

$$\kappa_X = \frac{M_4}{\sigma_X^4} = \frac{E[(x - \mu_X)^4]}{\sigma_X^4}, \tag{11}$$

where σ_X is the standard deviation of X .

It is obvious from Eq. (7) that the moments of odd order are all zero if the PDF $f_X(x)$ is even. For example, the commonly used Gaussian or normal distribution has the skewness $S_X = 0.0$ and the kurtosis $\kappa_X = 3.0$. In fact, the two moments can be used as indices to test how far a random variable deviates from Gaussian normal. In addition, the kurtosis coefficient can be applied to classify the system non-linearities if the systems are non-memory [16]. For that reason, these two statistical moments draw much less attention in real applications even within cases of the Gaussian distribution. However, let the random signal X be first rectified to one-side in such a way that

$$Y(t) = |X(t)|. \tag{12}$$

Then the value of the skewness will definitely be non-zero, while the kurtosis is the same. For example, the first rectified moment

$$\mu_Y = \frac{1}{N} \sum_{i=1}^N |x_i|, \quad (13)$$

which will never be zero unless all x_i are zero. As the calculation shows [17], $S_Y = 1.6$ and $\kappa_Y = \kappa_X = 3.0$ for the Gaussian distribution. And thus depending on the signal amplitudes, σ_Y , S_Y and κ_Y in addition to μ_Y , are chosen as the input signals for the current study.

4. Experimental setups

Fig. 2 shows the block diagram of the experimental process. The acoustic signals of a rotary disk were generated from the PBS-5000 rotor kit in the lab. The phenomenon signals of both normal and malfunction were purposely generated depending on the needs of analysis by means of this rotor kit. For example, a known extra mass is put on a well-balanced disk to simulate the mass unbalance of the machine. Moreover, the pre-processed signal data are randomly and evenly divided into two sets. One set is for the system training, while the other one is for diagnosis testing of the ANN. Refer to Fig. 2 for details.

The microphone that is installed close to one of the two bearings detects the acoustic signal generated from the machine. Meanwhile, the vibrations are acquired by and four non-contact proximity probes installed close to the two supporting bearings. For comparison, refer to Fig. 3. Both acoustic and vibration signals appear as a voltage and are adequately amplified before processing in the computer. In addition, in order to filter the DC voltage resulting from the initial installation of the probes, a second order Butter-Worth filter was added prior to the PCL-818H A/D card for vibration signals. The high-pass frequency was set at 5 Hz to get rid of the DC voltage while the lower-pass filter is at 1 kHz to filter those useless high-frequency signals and noise. The A/D card supplied by Advent Tech. Co. has 16 channels with the maximum sample rate of

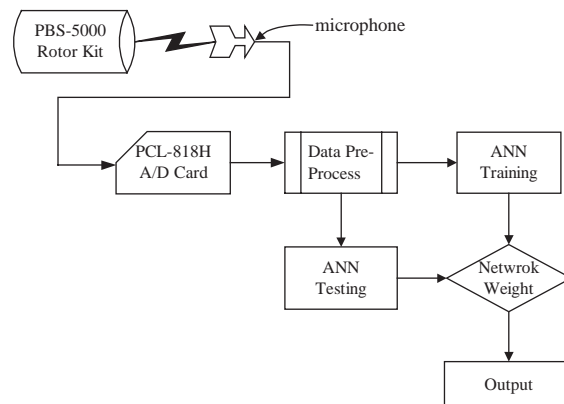


Fig. 2. Block diagram of the experiment system.

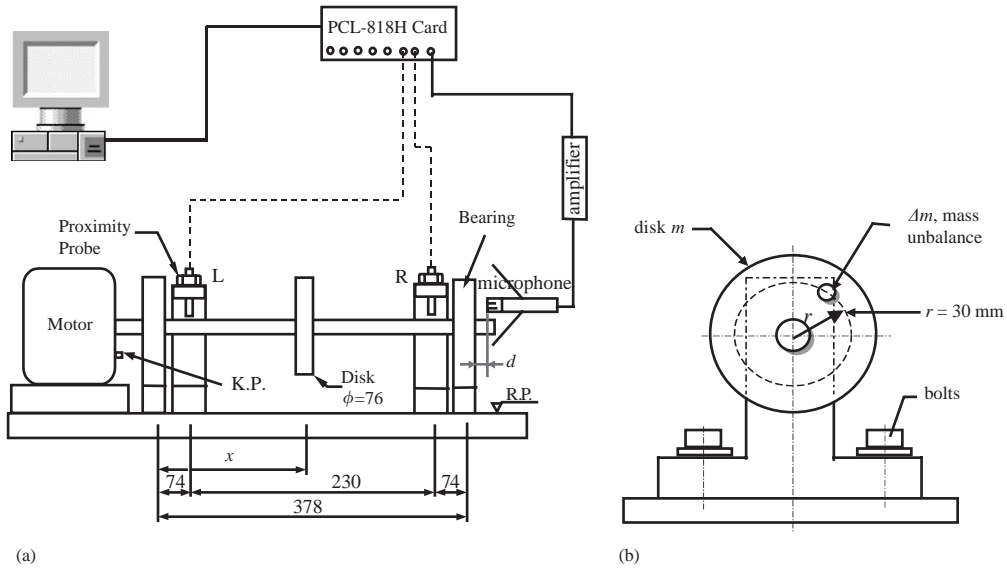


Fig. 3. (a) The experimental setup: microphone and the probe installations and (b) side view of the disk.

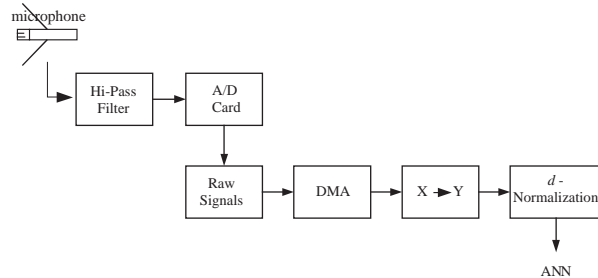


Fig. 4. Block diagram for signal processing.

10 MHz. Therefore, it is more than enough to acquire both the low-frequency vibration and acoustic signals of high frequencies. The signals collected from the A/D card are then digitized and stored in the PC for the next ANN training as well as testing.

The perturbation rotor kit is driven by a 3ϕ , 90 W AC motor. The shaft was made from high carbon steel with 9.525 mm ($\frac{3}{8}$ in) diameter and 276 g and coupled with the motor by a flexible coupling. The relative locations of the proximity probes and test disk (mass 411 g) are shown in Fig. 3 in addition to the microphone. Two proximity probes that were installed in the vertical and horizontal directions, 90° apart at the frame on the relative plane (RP) are shown in Fig. 3(b). The scale factor of the probes is 200 mv/mil up to 10 kHz with accuracy $\pm 4\%$.

Besides, there is an additional probe, or the so-called key phasor (KP), mounted on the RP to lock an impulsive signal in each shaft revolution. The signal from this KP probe will get the right rpm for the diagnosis system. See Fig. 4 for details of the experimental setup. Note that there are

six (6) channels which have been connected during the experiment. They are: one for the KP, one for the microphone, and the two proximity probes for each bearing.

5. Experiments

The main concern of the present study is the signals acquired from the microphone, even though there are four other proximity probes. The maximum sampling rate of the microphone was set to 8196 Hz, while only those signals below approximately 4 kHz were of interest. The total sampling time was set to 1.2 s. Thus, the frequency resolution is 1 Hz. In addition, the averaging method was applied to reduce the random noise. Both normal and abnormal signals were recorded for analysis. In addition, the signals were taken with various rotation speeds. For each speed, 20 samples were taken for processing later.

Anticipating for both training and test needs, the acquired acoustic signals were processed into those in the power spectra (P) and rectified statistical moments (S) introduced in Section 3. In addition, since the configuration of the rotor kit bearing has seven (7) balls inside the inner cage, some signals that are in fractions and multiples of seven are of main interest: 0.5ω , ω , 2ω , 3ω , 4ω , 5ω , 6ω , and 3.5ω , 7ω , 14ω and 21ω . Here, ω stands for the speed of the disk. It can be either in Hz or in RPM. Nevertheless, there are 11 intensity feature inputs in the frequency domain to be fed into the ANN. More than that, there are four features in S including μ_Y , σ_Y , S_Y , and κ_Y .

Since the acoustic signals are recorded from the microphone, one crucial factor that affects the quality of the ANN is the distance. That is, the effect of the distance between the microphone and the acoustic source, shown by ' d ' in Fig. 3(a), has to be successfully eliminated, otherwise, the input would be meaningless since the sound intensity attenuates as the distance increases. In order to normalize those acoustic signals, a d -normalization was designed for readers who are into speech synthesis may be familiar with the loudness or acoustic volume of speech, e.g., [16]. Analogous to that definition of the acoustic volume function, the row acoustic signals can be normalized by dividing by μ_Y , or, referring to Fig. 4. Let $I^*(f)$ be the sound intensity power at a frequency f . Then the d -normalization was defined by

$$I(f) = \frac{I^*(f)}{\mu_Y}, \quad (14)$$

where μ_Y has been defined in Eq. (13). Fig. 5 compares a typical acoustic power spectrum before and after the d -normalization. The figure shows that the distance between the microphone and the acoustic source has been successfully reduced to a very low level.

Furthermore, the output signals are normalized in another way. That is, let $\mathbf{y}^* = \{y_1^*, y_2^*, \dots, y_r^*\}^T$ be the output vector before normalization. Then it can be normalized by its one-norm by

$$\mathbf{y} = \frac{\mathbf{y}^*}{\|\mathbf{y}^*\|_1} = \frac{\{y_1^*, y_2^*, \dots, y_r^*\}^T}{\sum_{i=1}^r |y_i^*|}. \quad (15)$$

The normalized output vector \mathbf{y} is then compared with the target vector \mathbf{T} in the ANN training. Besides, in the present study, the length of the output vector \mathbf{y} is 4, i.e., $r = 4$.

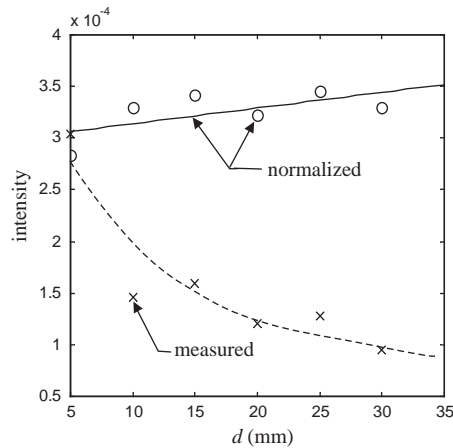


Fig. 5. Normalized acoustic intensities ('x': before normalization, 'o': after d -normalization) for $\omega = 60$ Hz.

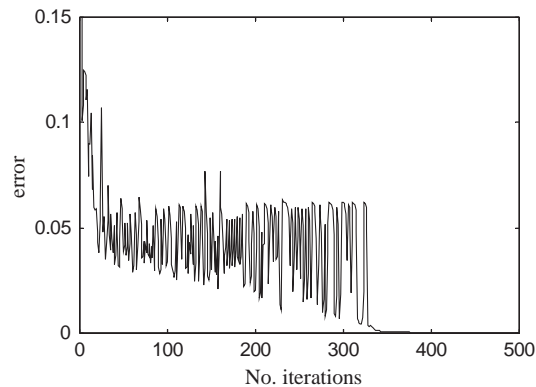


Fig. 6. Maximum cumulative error (ϵ_{max}) of ANN for acoustic inputs.

6. Results and discussions

As mentioned earlier, the ANN parameters are very important and affect its performance [2–7]. For example, the momentum factor (ω) was set to a fixed value of 0.9 in addition to N_{in} : N_H : $r = 16:10:4$, and, the maximum iterations was 2000 in case $\epsilon_{max} = 0.002$ (0.2%) could not be reached. In addition, the learning rate constant of 0.3 was selected for the current ANN. Fig. 6 shows the residual error during the network training. Note that the levels of ϵ_{max} are too small to be seen in the figure.

The unbalance was established by adding 0.25% extra mass to the disk, i.e., $\Delta m/m = 0.7/276$ g, during the experiments. For reasons of comparison, the signals were acquired both by using the proximity probes and the microphone. Figs. 7 and 8 show the two signals recorded from the two different sensors for rotation speed $\omega = 60$ Hz and at the normal condition $\Delta m = 0$. Despite the intensities of the two signals in these two plots, they are actually consistent, especially at 1ω . However, the acoustic signals seem to have more harmonic peaks than that of proximity probes.

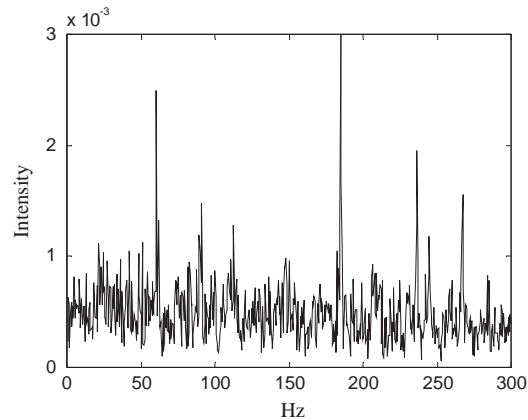


Fig. 7. Normal at $\omega = 60$ Hz with acoustic signals.

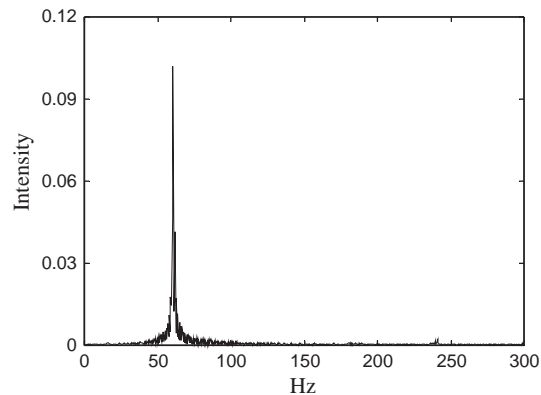
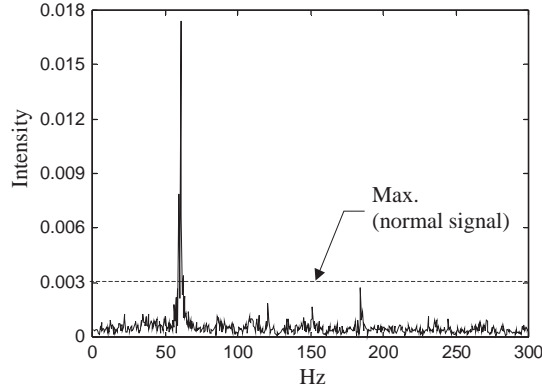


Fig. 8. Normal at $\omega = 60$ Hz with proximity probe signals.

For instance, there is the highest peak at 3ω (180 Hz) in Fig. 7, but not in Fig. 8. Note, the proximity probes were to measure the amount of the axis oscillations including shaft bow, while the microphone was put close the right bearing. In other words, the latter may further include defects of the bearings. That may be the reason the latter has more peaks in Fig. 7. Nevertheless, the acoustic signals seem to have more information than the proximity probes.

Fig. 9 shows the acoustic signals in the case where unbalance $\Delta m = 0.7$ g. As can be clearly seen by comparing Figs. 9 and 7, the extra unbalance mass creates much larger acoustic power right at 1ω . However, as one can see from Fig. 9 the acoustic intensity at 3ω did not increase proportionally. Instead, it became much small relatively to that of the power unbalance mass at 1ω . Note that the approximate maximum level of normal condition has also been plotted in Fig. 9 for comparison.

For convenience of expression, the braces ($\{\cdot\cdot\}$) denote the rotational speeds inside the braces, while those in the brackets ($[\cdot\cdot]$) are the speed ranges analogous to math symbols. For example, ‘{30, 50} Hz’ means the speeds at 30 and 50 Hz.

Fig. 9. Acoustic signals for unbalance of 0.25% at $\omega = 60$ Hz.Table 1
Constant speed tests in [30, 100] Hz

Disk rpm (Hz)	30	40	50	60
Train/test samples	40/40	40/40	40/40	40/40
Results (%)	100	90	100	100
Disk rpm (Hz)	70	80	90	100
Train/test samples	40/40	40/40	40/40	40/40
Results (%)	100	100	100	100

Under the constant speed test, the ANN was trained with acoustic signals acquired in [30, 100] Hz under the same unbalance condition. After the ANN converged below the acceptable error level, it was tested by signals of $\omega \pm \Delta\omega$, i.e., the test signals were generated in the vicinity of the training speed. By doing so, the ANN may be more flexible and robust in real application. The results are shown in Table 1. With $\Delta\omega = 2.5$ Hz, the ANN is able to 100% classify the cases of normal and abnormal, with the exception at $\omega = 40$ Hz.

It can be seen from Table 1 that the ANN cannot identify the machine condition at rotational speed at $\omega = 40$ Hz. As has been shown in [17], the rotor disk was purposely set to process the first natural frequency approximately at 80 Hz. On the other hand, the configuration of the ball bearing is depicted in Fig. 10. Assuming there exist no slipping at the ball and fixed the outer ring, one has no difficulty in finding the velocity of the inner ring as [9]

$$V_{in} = \omega \cdot R_{in}, \quad (16)$$

while for the outer ring $V_{out} = 0$, refer to Fig. 10; and, the ball center has velocity V_b ,

$$V_b = \frac{1}{2}\omega \cdot R_{in}. \quad (17)$$

In addition, the retaining cage which locates at $R_B = (R_{in} + R_{out})/2$, has the same velocity as the balls. In fact the cage acts in such a way as to keep all rolling balls in the same motion. Thus, the

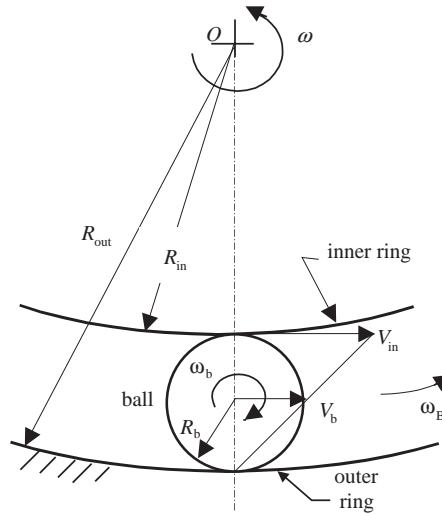


Fig. 10. Anti-friction ball bearing.

angular velocity of the rolling set, including the balls and the cage, is

$$\omega_B = \frac{V_b}{R_B} = \frac{\frac{1}{2}\omega \cdot R_{in}}{\frac{1}{2}(R_{in} + R_{out})} = \left(\frac{R_{in}}{R_{in} + R_{out}} \right) \omega. \quad (18)$$

Eq. (18) actually implies that the rolling sets of the rotor kit generate signals at a frequency less than and close to $\omega/2$ if the shaft rotates with the angular velocity of ω .

In addition, it is clear that there exist quadratic non-linearities in the rotor-disk system, e.g., [18]. As a consequence, the energy excited at $\omega = 40$ Hz flows into 2ω , which is 80 Hz, as shown in Fig. 11(a) and (b). This phenomenon has been known and classified as internal resonance [19,20]. In other words, if in non-linear system natural frequencies satisfy $\omega_i = 2\omega_j$, for some i and j , then the system energy may flow forth back and between these two modes. As one can read by comparing Fig. 11(a) and (b), such energy leaks to 2ω (80 Hz) happen at both unbalance and normal conditions. As a result, the ANN can hardly classify the difference between normal and abnormal condition at this speed.

Similarly, in the case where $\omega = 80$ Hz is excited, the system energy again flows to 40 Hz too. However, the results from Table 1 show that the ANN can successfully identify the signals at this speed, even if the speed is very close to the disk resonance. The main reason stems from the fact that the training set of the ANN has included signals of that particular non-linear phenomenon. Moreover, the signals of the unbalance mass at $\omega = 80$ Hz are so strong that the ANN can easily identify the features.

Fig. 12 shows the same acoustic power as in the case of Fig. 11(a). The energy flows into 2ω is very clear, that is, the same as in Fig. 11(a), though all other multiples of ω include more noises. In addition, there exist some other unknown peaks in the spectra. It is the authors' opinion that these strange peaks mainly stem from the imperfectness of ball bearings or its cage.

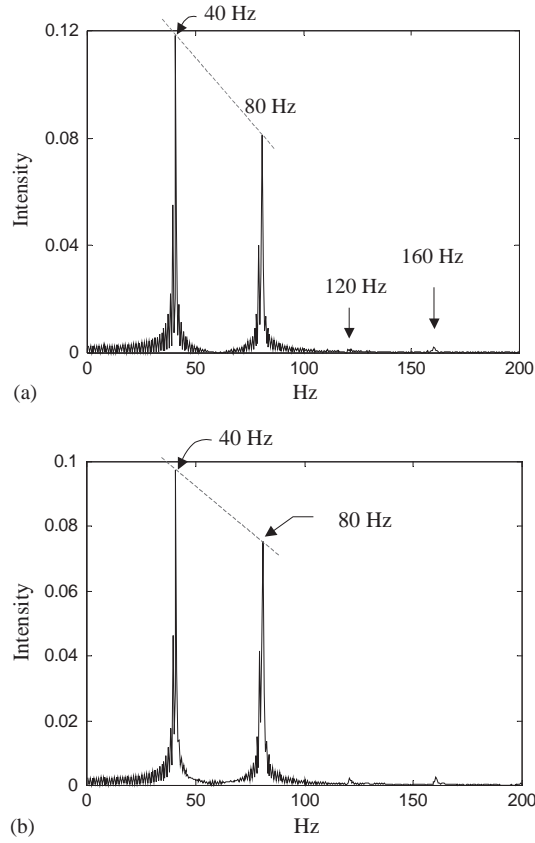


Fig. 11. Vibration signals at $\omega = 40$ Hz for: (a) unbalance of 0.25% and (b) normal condition.

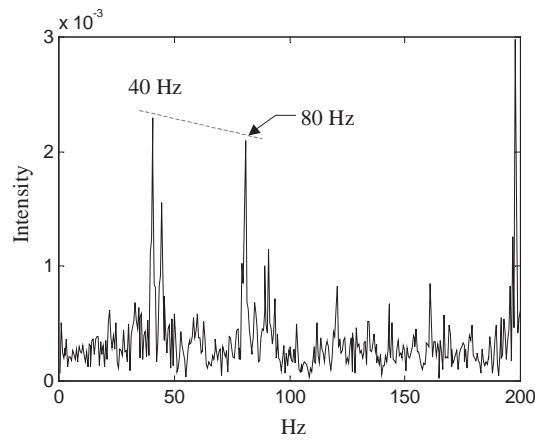


Fig. 12. Acoustic signals for unbalance of 0.25% at $\omega = 40$ Hz.

7. Conclusions

A diagnosis expert system for identifying the mass unbalance of rotating machines was developed and tested in the present study. The expert system adopts the backward propagation neural network as the inference mechanism. The main feature inputs are extracted from the signals that are acquired by a microphone. The acoustic signals are better than the traditional vibrations because of the mobility of the sensors. However, the distance between the microphone and the acoustic source is the main factor that affects the quality of the input feature. This problem can be overcome by the so-called *d*-normalization before putting into the system. The ‘*d*-normalization’ is actually similar to the normalization based on the loudness or the acoustic volume. Nevertheless, the experimental study showed that the *d*-normalization could successfully minimize the effect of the source distance.

In addition, the acoustic power spectra together with rectified statistical moments were designed as the major input representations for the expert system. Both the skewness and kurtosis coefficients are sensitive to the change of rotating speeds or signal amplitudes. And, thus they can provide additional information as long as the malfunctioning signal deviates from the normal one. Moreover, the first moment of the rectified acoustic signals can be used as the base of *d*-normalization.

The system was further verified by many tests under different considerations. It has been found that the ANN system is good except that there exists a special phenomenon like resonance.

Acknowledgements

The financial support of the present research from the National Science Council (NSC) of Taiwan under NSC-89-2212-E-027-006 is thankfully acknowledged.

References

- [1] P.R. Drake, D. Pan, Multiple fault diagnosis for a machine tool's flood coolant system using a neural network, *International Journal of Production Research* 30 (4) (1992) 825–837.
- [2] L.D. Zhao, Z.H. Sheng, Combination of discrete cosine transform with neural network in fault diagnosis for rotating machinery, *IEEE Transactions on Industrial Technology*, 1996, pp. 450–454.
- [3] H.H. Huang, H.P.B. Wang, An integrated monitoring and diagnostic system for roller bearings, *International Journal of Advanced Manufacturing Technology* 11 (12) (1996) 37–46.
- [4] T.I. Liu, N.R. Iyer, Diagnosis of roller bearing defects using neural network, *International Advanced Manufacturing Technology* 8 (4) (1993) 252–257.
- [5] I.E. Alguindigue, A. Loskiewicz-Buczak, R. Uhrig, Monitoring and diagnosis for rolling element bearings using artificial neural networks, *IEEE Transactions on Industrial Electronics* 40 (2) (1993) 209–217.
- [6] P.J. Werbos, Back-propagation through time: what it does and how to do it, in: M.M. Gupta, D.H. Rao, (Eds.), *Neural Control Systems, Theory and Applications*, IEEE Press, New York, 1994, pp. 297–307.
- [7] Z.-C. Lin, C.-Y. Hsu, Tech. An investigation of an expert system for shearing cut progressive die design, *International Journal of Advanced Manufacturing Technology* 11 (1) (1996) 1–11.
- [8] W. Li, et al., Study on plot identification of vibration signals using an expert system, TPC research report, 1997 (in Chinese).
- [9] C.L. Chiu, An Expert System Based on Acoustic Inputs, Master's Thesis, NTUT, Taipei, 2001 (in Chinese).

- [10] M. Hagiwara, Theoretical derivation of a momentum term in back-propagation, *International Joint Conference on Neural Networks*, Vol. 1, 1992, pp. 682–686.
- [11] S. Haykin, *Neural Networks: a Comprehensive Foundation*, Prentice-Hall, Englewood Cliffs, NJ, 1994.
- [12] L.V. Fausett, *Fundamentals of Neural Network: Architectures Algorithms and Applications*, Prentice-Hall, Englewood Cliffs, NJ, 1994.
- [13] F. Honarver, H.R. Martin, New statistical moments for diagnostics of rolling element bearings, *Journal of Manufacturing and Science Engineering Transactions ASME* 119 (1997) 425–432.
- [14] W. Li, S.S. Chang, An artificial neural network system for machinery diagnoses using statistical moments as auxiliary inputs, *Proceedings ICMT98*, Hsinchu, Taiwan, 1998, pp. 513–518.
- [15] A. Nadi, et al., Classification of condition of rotating machines using higher order statistics, *IEEE Colloquium on Higher Order Statistics in Signal Processing*, 1995, pp. 3/1–3/6.
- [16] D.G. Childers, *Speech Processing, Synthesis Toolboxes*, Wiley, New York, 2000, p. 337.
- [17] W. Li, J.J. Gau, The effects of selections of training signals to a BPN neural network for automatic environmental tests, *Proceedings of the 11th Automation Conference*, Taipei, Taiwan, 1999.
- [18] D. Childs, *Turbomachinery Rotordynamics*, Wiley, New York, 1993, p. 2.
- [19] R.M. Evan-Iwanowski, *Resonance Oscillations in Mechanical Systems*, Elsevier, Amsterdam, 1976, p. 44.
- [20] W. Li, R.A. Ibrahim, Principal internal resonance in 3-DOF systems subjected to wide-band random excitations, *Journal of Sound and Vibration* 131 (2) (1989) 305–321.